Rapid Current Ramp-Up by Cyclotron-Driving Electrons beyond Runaway Velocity

M. Uchida, T. Yoshinaga,* H. Tanaka, and T. Maekawa
Graduate School of Energy Science, Kyoto University, Kyoto 606-8502, Japan
(Received 3 May 2009; published 8 February 2010)

The toroidal current has been rapidly ramped-up after the formation of an initial closed flux surface in an electron cyclotron heated discharge in the low aspect ratio torus experiment device. A current carrying fast electron tail is developed well beyond the runaway velocity against the reverse voltage from self-induction, suggesting a forward driving force on the tail by the cyclotron absorption of high $N_{\|}$ electron Bernstein waves.

DOI: 10.1103/PhysRevLett.104.065001 PACS numbers: 52.50.Sw, 52.35.Hr, 52.55.Fa, 52.55.Wq

The toroidal plasma current in tokamaks keeps the plasma loop in equilibrium and forms nested magnetic surfaces for confinement. Usually it is initiated, ramped-up, and maintained by induction from a central solenoid (CS). If the CS can be removed, the structure of future tokamak reactors will be greatly simplified and the aspect ratio of the torus will be reduced, which is beneficial to keeping fusion plasma at a lower toroidal magnetic field (MF) [1].

Various methods of noninductive current drive were proposed and investigated to remove CS [2]. Among them, microwave injections at the electron cyclotron (EC) range of frequency are especially advantageous for reactors [3,4], since the microwave beam can be injected from a small launcher remote from the plasma. The EC method has been useful for the formation of initial plasma [5] and initial magnetic surface [6–9]. While steady current maintenance was also realized in a number of experiments [3,4,10,11], plasma current was initially ramped-up by CS and then the driver switched to the EC power. With current ramp-up by EC power whole process from plasma initiation to final tokamak plasma formation could be covered solely by one EC system.

In the EC current maintenance, a group of tail electrons traveling along the MF lines at several times the thermal speed are selectively heated nearly perpendicularly to MF at the Doppler-shifted EC resonance frequencies. More precisely, each resonance electron gains a parallel momentum and an energy from the waves at the ratio $\delta p_{\|}/\delta\mathcal{E} = N_{\|}/c$ [2] ($N_{\|}$ is the parallel refractive index along MF). Hence, the power deposition induces a flow toward higher velocity region in the velocity space. Since the collisional relaxation time of tail electrons becomes longer with velocity, the flow builds up a unidirectional extra population over the background Maxwellian tail, resulting in a steady current.

In the current ramp-up case, there arises an electric (E) field from self-induction, exerting another counterforce to electrons in addition to the collisional force. We introduce the runaway velocity $v_R = \sqrt{m\Gamma/|qE|}$ at which both forces becomes equal [2]. Here $\Gamma = n_e q^4 \ln\Lambda/4\pi\epsilon_0^2 m^2$, and m and q are the electron mass and charge, respectively. It is essential for effective current ramp-up to build up current carrying fast electrons in the velocity range well beyond v_R, where collisional force rapidly falls off with velocity as v^{-2} and the E force alone exerts on the fast electrons. The work done by the fast electrons against the E force is converted to the magnetic energy of the current loop.

In this Letter, we report an experiment in which plasma current rapidly ramps up as fast as ~260 kA/s by EC power, being much faster than previous results (2–50 kA/s) [10,12] and comparable to the lower hybrid ramp-up rate (120–240 kA/s) [13,14]. This rapidly ramping-up current is found to be carried by energetic passing (i.e., fast) electrons in the velocity range well beyond v_R. This important regime of EC current drive is obtained for the first time, shedding a light to start-up tokamak fusion plasma without CS. The wave overdrives electrons from the thermal tail toward the energetic range against the counter E force. The driving force may originate from the cyclotron absorption of high $N_{\|}$ electron Bernstein (EB) waves since the parallel momentum input to resonance electrons is proportional to $N_{\|}$. Note that EB waves are an electrostatic mode and can have high $N_{\|}$ while the electromagnetic (EM) modes cannot.

The experiment was carried out in the low aspect ratio torus experiment (LATE) device [12]. The vacuum chamber is a cylinder with a center post [see Fig. 1(h)]. There is no CS for inductive current drive. Microwave at 5 GHz with an injection power of $P_{\mathrm{rf}} \simeq 190$ kW is launched obliquely to the toroidal field via a cylindrical launcher of open waveguide type on the midplane.

Figure 1 shows a typical current ramp-up discharge. The vacuum chamber is prefilled with hydrogen gas at $p \simeq 7 \times 10^{-3}$ Pa under a steady helical field line of a vertical field of $B_v = 70$ G and a toroidal field of $B_t = 960$ G (all at $R = 25$ cm). When a 5 GHz microwave pulse is turned on, breakdown takes place immediately along the external helical field lines near the 2nd EC resonance layer at $R = 27$ cm [Fig. 1(f)]. After a while, plasma current jumps up to 7 kA under the steady B_v field [Fig. 1(a)], spontaneously forming an initial closed field structure [Fig. 1(g)] as described in the previous Letter [7]. This is the first stage

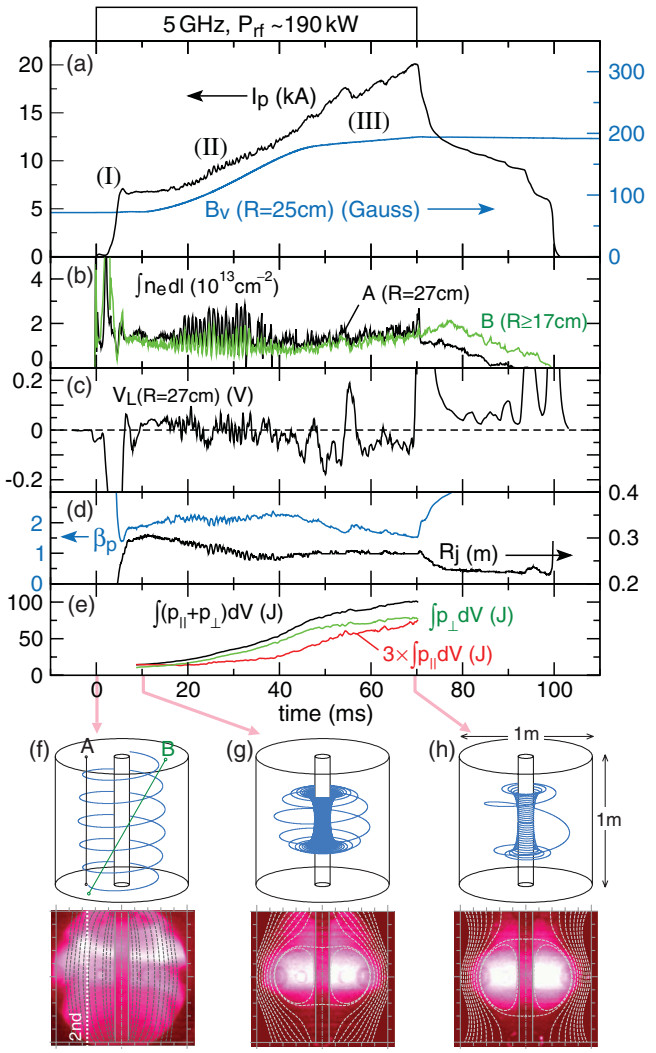

FIG. 1 (color). A 20 kA current ramp-up discharge (a) plasma current and B_v; (b) line densities along chords A and B [see (f)]; (c) loop voltage at the plasma core; (d) beta-poloidal and radial current center; (e) volume integrals of parallel and perpendicular pressures. (f), (g), and (h) Field lines and plasma images at the breakdown, initial closed field formation and final low aspect ratio torus formation, respectively.

denoted by (I) in Fig. 1(a). In the next stage (II), I_p ramps up as B_v is ramped-up. At the final stage (III), where B_v ramp-up rate is turned very low, I_p still ramps-up at the same rate of ~260 kA/s as the stage (II) against the reverse loop voltage V_L appeared in this stage [Fig. 1(c)]. I_p finally reaches 20 kA at the end of microwave pulse, producing a low aspect ratio torus [Fig. 1(h)]. The last stage (III) constitutes the new regime and is fully described below.

Data from 17 flux loops have been used for the estimation of the plasma current profile [15]. We have taken into account eddy currents induced in the vacuum vessel. The profile model has been, however, improved from that in [15]. It assumes a power law parabolic profile with eight fitting parameters to the flux signals including newly employed parameters of triangularity (δ) and radial shift of current peak (σ). The fitted result at $I_p = 20$ kA in Fig. 1 is shown in Fig. 2(a). The difference between the flux signals and the fitted ones is improved to be typically less than 1% due to adjustments of δ and σ, while it was ~3% in the previous model [15].

The line averaged electron density is estimated from two chords measurements [Figs. 1(b) and 1(f)] to be $\bar{n}_e \simeq 4 \times 10^{11}$ cm^{-3} at stage (III). This is higher than the plasma cutoff density ($n_c = 3 \times 10^{11}$ cm^{-3}), suggesting that EB waves mode-converted from the incident EM waves support the plasma and drive the current.

Visible light plasma images show that the plasma does not burn through the radiation barrier, indicating $T_e \lesssim 100$ eV. Then, contribution of the thermal electrons to

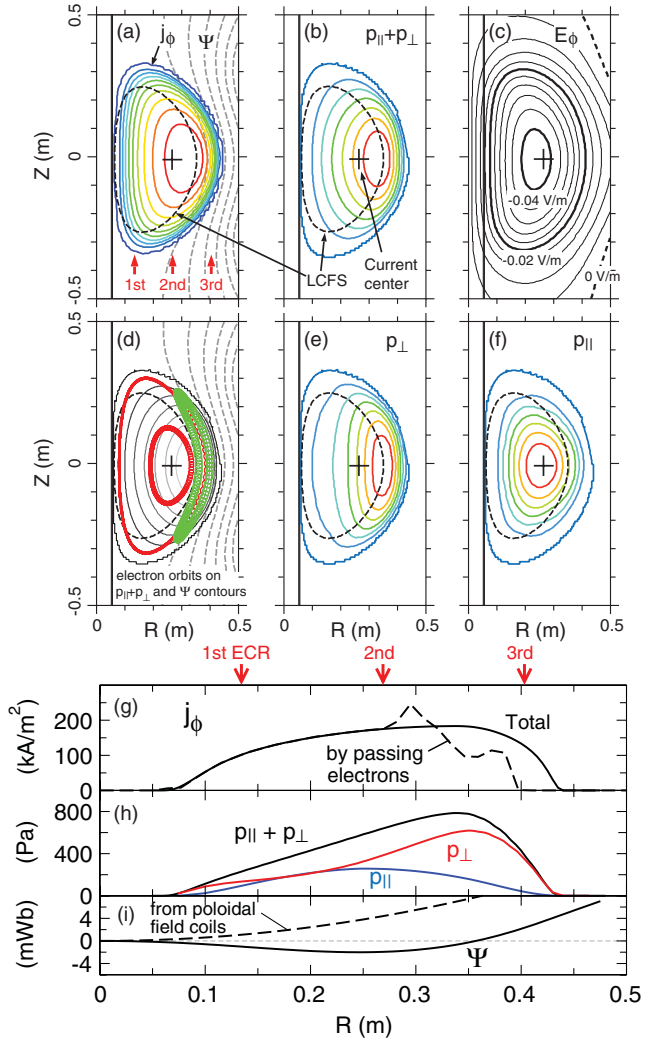

FIG. 2 (color). Profiles of various quantities of the 20 kA plasma in Fig. 1. (a) Toroidal current density and poloidal flux; (b) "sum" pressure; (c) toroidal electric field; (d) various orbits of 100 keV electrons; (e) perpendicular pressure and (f) parallel pressure on the poloidal cross section; and (g), (h), and (i) their radial profiles on the midplane. Contours are equally spaced.

beta-poloidal, $\beta_{p_{\rm th}} = 8\pi S\langle p_{\rm th}\rangle/\mu_0 I_p^2$ ($p_{\rm th} \equiv n_e T_e$, S is the cross section and $\langle\,\rangle$ denotes the average over S) is estimated to be $\beta_{p_{\rm th}} \le 0.05$ by using $\bar{n}_e = 4 \times 10^{11}$ cm^{-3}, $S \approx 0.15$ m^2, and $I_p = 20$ kA. While β_p is estimated to be $\beta_p \approx 1.5$ [Fig. 1(d)] from the information on $\beta_p + l_i/2$ obtained by the magnetic analysis [16] and on the internal inductance l_i calculated from the fitted current profiles. This value is 30 times larger than the thermal contribution, indicating the presence of energetic electrons. Their presence is also shown by the evolution of hard x-ray energy spectra in Fig. 3. The energy range expands as I_p increases and is developed up to $\mathcal{E}_X \sim 200$ keV when $I_p \sim 15$ kA. Thus, there are two groups of electrons, thermal electrons and energetic electrons. While the latter is a few percent in population as estimated by $(\beta_p/\mathcal{E}_X)/(\beta_{p_{\rm th}}/T_e)$, it dominates in pressure and carries the current since $p_{\rm th}$, T_e, and V_L [Fig. 1(c)] are low and contributions from thermal electrons are negligible.

The radial force balance of a plasma torus may be described by the following generalized Shafranov formula:

$$R_0 I_p B_v = \frac{\mu_0}{4\pi} G(R_0/a, \kappa, l_i, \text{etc}) I_p^2 + 2S\langle p\rangle. \qquad (1)$$

The first term of the right side represents the current loop expanding force proportional to I_p^2 and the second term does the pressure ballooning force. In the original Shafranov formula [17], $G = \ln(8R_0/a) + l_i/2 - 3/2$. In the present case the formula may still hold with an appropriate G value that reflects low aspect ratio and noncircular cross section, etc.

Figure 4(a) illustrates the discharge evolution on the (I_p, $R_j B_v$) plane and also does the contour map of $S\langle p\rangle$ predicted by formula (1) as a function of I_p and $R_0 B_v$ with $G = 1.1$. Corresponding evolution of $S\langle p\rangle$ for the present discharge is obtained by using the magnetic analyses described above and the result is plotted as a function of I_p in Fig. 4(b) and compared with the prediction by formula (1) by assuming that $R_0 = R_j$, showing good consistency. Figure 4(b) shows that $S\langle p\rangle$ is proportional to I_p in stage (III) while it increases faster than I_p in (II). This behavior suggests that the energy range of energetic electrons becomes saturated in (III) while it increases with I_p in stage (II). In accordance with this behavior B_v ramp-up rate versus I_p is as low as $R_0 dB_v/dI_p = \mu_0 G/4\pi$ in (III) while it is much larger in (II) as shown in Fig. 4(a). In the last stage (III), therefore, the self-induction of plasma current dominates over the induction from B_v coil currents and the loop voltage at the plasma core becomes significantly negative as shown in Figs. 1(c) and 2(c). Typical energy of fast electrons is ~100 keV as shown later and much larger than the runaway energy, $mv_R^2/2 \lesssim 4$ keV for the present E field of $|E_\phi| \gtrsim 0.02$ V/m in this last stage, manifesting the new regime of EC current drive.

The current profile in Fig. 2(a) shows that the current outside the last closed flux surface (LCFS) is significant, indicating pressure gradients along the open field lines connected with the wall. The isotropic pressure does not support pressure gradients along field lines. Therefore, we study details of the local equilibrium by using the equation for anisotropic pressure; $\mathbf{j} \times \mathbf{B} = \nabla \cdot \mathsf{P}$, where $\mathsf{P} = p_\perp \mathsf{I} + (p_\parallel - p_\perp)\mathbf{bb}$ and $\mathbf{b} = \mathbf{B}/B$ is the unit vector along the field line, and, $p_\parallel \equiv n_e m\langle \gamma v_\parallel v_\parallel\rangle_v$ and $p_\perp \equiv n_e m\langle \gamma v_\perp v_\perp/2\rangle_v$ where γ is the relativistic factor, $\parallel$ and $\perp$ denote the parallel and perpendicular components to MF, respectively, and $\langle\,\rangle_v$ the average over the velocity space. In the cylindrical coordinates (R, ϕ, Z) with Z axis being the axisymmetric axis of the torus, the radial and vertical components of the equation are approximately given by $j_\phi B_Z - j_Z B_\phi = \partial p_\perp/\partial R + (p_\perp - p_\parallel)/R$ and $j_R B_\phi - j_\phi B_R = \partial p_\perp/\partial Z$, respectively, by neglecting small correction terms proportional to $\sin^2\alpha$ (α is the angle between the field line and the toroidal direction). By combining these equations with the constraint on currents, $\nabla \cdot \mathbf{j} = 0$, we have $\partial(p_\perp + p_\parallel)/\partial Z = -2j_\phi B_R - R\partial(j_\phi B_Z)/\partial Z - R\partial(j_\phi B_R)/\partial R$, which gives the "sum"

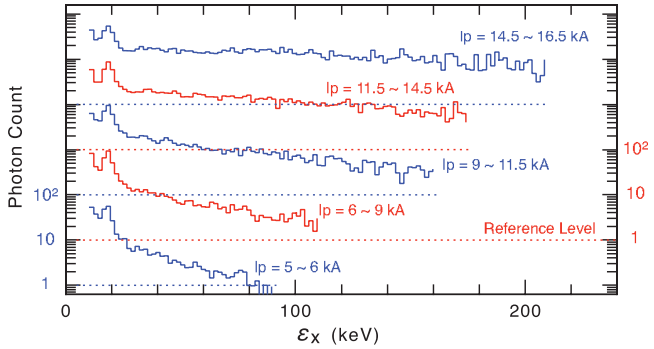

FIG. 3 (color). Hard x-ray energy spectra measured along a vertical chord at $R = 28$ cm $\sim R_j$ by a CdTe detector.

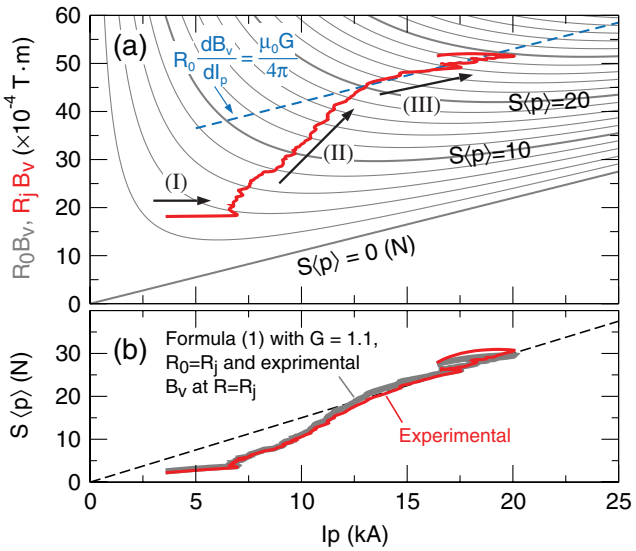

FIG. 4 (color). Plasma loop equilibrium. Red plots are characteristics of the 20 kA discharge in Fig. 1. Gray contours and plots are those predicted by formula (1) with $G = 1.1$.

pressure profile shown in Fig. 2(b). Finally, the toroidal component of the equilibrium equation resolves the sum pressure profile into the parallel and perpendicular pressure profiles as shown in Figs. 2(e) and 2(f).

The radial profiles of the current density, pressures, and poloidal flux on the midplane are plotted in Figs. 2(g)–2(i), respectively, showing that $p_{\parallel}$ is much smaller than $p_{\perp}$ outside the LCFS but becomes comparable at the inside. This result suggests that the inside current [it amounts to 67% of I_p in Fig. 2(a)] is carried mainly by passing electrons, while the outside current arises mainly as a result of the toroidal precession of trapped electrons. Field lines outside the LCFS have a large mirror ratio and provide mirror confinement for trapped electrons. Typical trajectories of these energetic electrons are plotted in Fig. 2(d), being consistent with the current and pressure profiles. There exist only passing electrons on the midplane at the inboard side of the magnetic axis. The profiles of j_{ϕ}, $p_{\perp}$, and $p_{\parallel}$ on this plane contain information on the pitch angle and energy range of passing electrons that circle around the torus. A measure for the ratio of passing electron current to I_p is estimated by assuming a monochromatic velocity distribution both in velocity and pitch angle. The current density over the poloidal cross section by these monochromatic passing electrons is obtained by tracing out a large number of trajectories starting from evenly distributed points on the inboard midplane. In the case that there are no backward passing electrons, the result is 70%. In the case of 20% backward to forward electrons, it amounts to 75% of I_p. These estimations suggest that main part of I_p is carried by passing electrons (fast electrons). The current profile on the midplane in the latter case is plotted in Fig. 2(g), where typical energy, pitch angle and density of the monochromatic fast electrons are 100 keV, 60°, and 10^{10} cm^{-3}, respectively.

After the end of stage (II), $\int p_{\parallel} dV$ increases faster than $\int p_{\perp} dV$ as shown in Fig. 1(e), indicating that the passing component increases faster than the trapping one. Furthermore, the V_L spike and I_p drop at $t = 54.5$–56 ms is coincident with the temporal decline of $\int p_{\parallel} dV$ and increment of $\int p_{\perp} dV$, suggesting a transient redistribution of pitch angles of fast electrons. Such a phenomenon was often observed in runaway discharges and attributed to the instability inherent for extremely deformed velocity distributions at the runaway energy range [18].

The diameter of the launcher is only twice the free space wavelength and the waves spread from the launcher with a wide $N_{\parallel}$ spectrum. Because of the conservation of toroidal mode number the $N_{\parallel}$ spectrum upshifts as the waves propagate toward inside, being inversely proportional to R. This effect is large in the present low aspect ratio plasma. Thus, a fractional part of incident waves may be converted to high $N_{\parallel}$ waves at the plasma core. Figure 5 shows the case where $N_{\parallel}$ upshifts as R^{-1} toward the EC resonance layer. The quasilinear diffusion arrows make a path in the velocity space that leads thermal electrons to the forward high energy region, resulting in the formation of the fast electron tail described above.

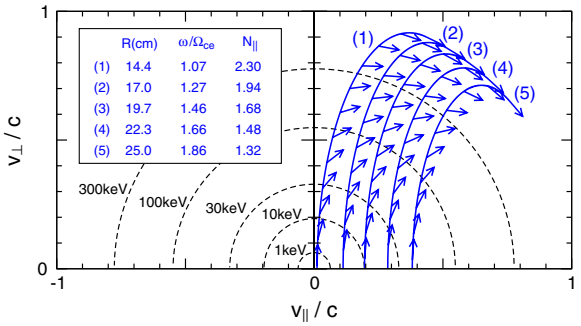

FIG. 5 (color online). EC resonance ellipses for high $N_{\parallel}$ waves. Arrow denotes the directions of quasilinear diffusion by the EC resonance absorption. Relativistic results.

For the same discharges as Fig. 1 total heat load to the limiters was measured to be 20%–50% of P_{rf}, which was mainly due to fast electron losses. Thus, the spatial loss is overwhelmingly large in the present small device [4] and conversion efficiency from P_{rf} to the poloidal MF energy is not high. In spite of these limitations in the wave launch and confinement present experiment has shown that EC driven fast electron tail is effective for current ramp-up. In large devices with no such limitations efficient current ramp-up would be expected. The work was supported by the KAKENHI and NIFS collaborative research program in Japan.

*Present Address: National Institute for Fusion Science, Toki, Gifu 509-5292, Japan

[1] M. Ono *et al.*, Nucl. Fusion **44**, 452 (2004).
[2] N. J. Fisch, Rev. Mod. Phys. **59**, 175 (1987).
[3] R. Prater, Phys. Plasmas **11**, 2349 (2004).
[4] T. C. Luce, IEEE Trans. Plasma Sci. **30**, 734 (2002).
[5] B. Lloyd *et al.*, Nucl. Fusion **31**, 2031 (1991).
[6] C. B. Forest *et al.*, Phys. Plasmas **1**, 1568 (1994).
[7] T. Yoshinaga, M. Uchida, H. Tanaka, and T. Maekawa, Phys. Rev. Lett. **96**, 125005 (2006).
[8] M. Gryaznevich, V. Shevchenko, and A. Sykes, Nucl. Fusion **46**, S573 (2006).
[9] A. Ejiri *et al.*, Nucl. Fusion **46**, 709 (2006).
[10] H. Tanaka *et al.*, Phys. Rev. Lett. **60**, 1033 (1988).
[11] S. Coda *et al.*, Plasma Phys. Controlled Fusion **42**, B311 (2000).
[12] T. Maekawa *et al.*, Nucl. Fusion **45**, 1439 (2005).
[13] F. C. Jobes *et al.*, Phys. Rev. Lett. **55**, 1295 (1985).
[14] Y. Takase *et al.*, Phys. Fluids **30**, 1169 (1987).
[15] T. Yoshinaga *et al.*, Nucl. Fusion **47**, 210 (2007).
[16] V. D. Shafranov, Plasma Phys. **13**, 757 (1971).
[17] V. D. Shafranov, in *Review of Plasma Physics* (Consultants Bureau, New York, 1966), Vol. 2.
[18] H. Knoepfel and D. A. Spong, Nucl. Fusion **19**, 785 (1979).